Microgravity Science and Technology (2018) 30:885–897
https://doi.org/10.1007/s12217-018-9651-4

ORIGINAL ARTICLE

Control of Rayleigh-Bénard Convection in a Fluid Layer with Internal Heat Generation

Z. Alloui[1] · Y. Alloui[2] · P. Vasseur[3]

Received: 10 June 2018 / Accepted: 20 August 2018 / Published online: 27 August 2018

Abstract

The control of the onset of convection in a horizontal fluid layer with internal heat generation is studied. The horizontal boundaries of the system are cooled isothermally. The stability of the fluid layer is investigated on the basis of the linear stability theory and the resulting eigenvalues problem is solved numerically. Upon using a feedback proportional control, the heating power of the system is modulated in order to counteract any deviations of the temperature of the fluid from its conductive value. As a result, it is possible to postpone (or advance) significantly the onset of motion. The optimal positions of the thermal sensors can be predicted on the basis of the linear stability theory. The linear stability analysis also reveals the possible existence of Hopf's bifurcations at the onset of motion. This type of bifurcation can be delayed using differential controllers. Two-dimensional numerical simulations of the full governing equations are carried out and found to agree well with the prediction of the linear stability theory.

Keywords Natural convection · Internal heat generation · Feedback control · Stability analysis

Nomenclature

A	aspect ratio of the cavity
a	wave number
C_p	specific heat at constant pressure of the fluid, $J/(kgK)$
D	differential operator, d/dy
E'	electric field magnitude, V/m
$\vec{g}$	gravitational acceleration, m/s^2
G'	proportional controller's gain, s^{-1}
G_t	differential controller's gain
k	thermal conductivity, $W/(m.K)$
L'	height of fluid layer, m
P'	pressure in the fluid layer, N/m^2
Pr	Prandtl number, υ/α
$\dot{q}'$	specific heating power, K/s
$\dot{q}'_E$	constant part of specific heating power, K/s
$\dot{q}'_A$	part of specific heating power supplied by the actuator, K/s
r	ratio between the controlled and uncontrolled critical Rayleigh number
Ra	Rayleigh number, $g\beta' \dot{q}'_E L'^5/\upsilon\alpha^2$
Ra_c	critical Rayleigh number
t'	time, s
T'	temperature in the fluid layer, K
$\vec{V}'$	velocity vector in fluid layer, m/s
x'	horizontal coordinate in fluid layer, m
y'	vertical coordinate in fluid layer, m
y'_s	vertical position of the temperature sensor, m

Greek symbols

α	thermal diffusivity of the fluid, m^2/s
β	thermal expansion coefficient, K^{-1}
μ	dynamic viscosity of fluid, Ns/m^2
υ	kinematic viscosity of fluid, m^2/s
ρ	density of fluid, kg/m^3
σ	electric conductivity, $\Omega^{-1}m^{-1}$

Subscript

c	critical condition
r	reference state
0	value at $y = 0$
1	value at $y = 1$

✉ Z. Alloui
z.alloui@univ-batna2.dz

[1] Département de Génie Mécanique, Faculté de Technologie, Université Mustapha Ben Boulaid Batna 2, 05000 Batna, Algérie

[2] Département de Génie Mécanique, Faculté des Sciences Appliquées, Université Kasdi Merbah Ouargla, 30000 Ouargla, Algérie

[3] Ecole Polytechnique, Université de Montréal, C.P. 6079, Succ. Centre Ville, Montréal, QC, H3C 3A7, Canada

Superscript

′ refers to dimensional variable

Introduction

Natural convection heat transfer in a plane horizontal layer subject to an adverse vertical temperature gradient has been a major topic of research in recent years. The interest is justified by its many applications such as meteorology, geophysics, astrophysics as well as in material processing technology in industrial applications. Since the pioneering works of Bénard (1900) and Rayleigh (1916) this flow configuration has been the object of numerous studies. A large cross section of fundamental research on this topic has been reviewed by Getling (1998).

Since convective flows are undesirable in many practical applications active suppression of onset of convection has potentially important applications in improving the material that goes through solidification in a mould. For instance, suppression or delay of onset of motion is desirable during Czochralski crystal growth (Muller 1988) in order to avoid inhomogeneities of dopants caused by convection during the growth process. One way to damp convective motions is the generation of a Lorentz force by applying a magnetic field in an electrically conducting fluid. It was demonstrated by Chandrasekhar (1961) that the effect of the Lorentz force, on the onset of motion in a horizontal layer heated from below, is to increase the value of the critical Rayleigh number and thus to have a stabilizing effect on the layer. The retardation effect of a magnetic field on the onset of Marangoni convection in a fluid layer with an upper free boundary was investigated first by Nield (1966). This study was extended by Maekawa and Tanasawa (1988) to consider the effect of orientation of the magnetic field. The influence of a vertical magnetic field on the onset of steady or oscillatory Marangoni convection was studied by Wilson (1993, 1994). Although these studies demonstrate the possibility for a magnetic field, to alter the stability characteristics in Rayleigh Bénard situations it is clear that this approach is only applicable to electrically conducting fluids. Another way to suppress convection is to take advantage of the weightless environment to reduce these motions (Delucas et al. 2002). However, the major handicaps of this technique are the scarcity of microgravity time and the cost.

Another way to delay the onset of convection is to employ active control, through perturbation of the thermal boundary conditions, to increase the stability threshold while maintaining a state of no motion in the fluid layer. The first study concerned with the active control of the Rayleigh-Bénard system seems to be due to Tang and Bau (1993, 1995). It was demonstrated theoretically by these authors that a simple control strategy, consisting in perturbing the lower boundary temperature (Tang and Bau 1993) or heat flux (Tang and Bau 1995), in proportion to the temperature at the mid-height of the fluid layer, can significantly retard the onset of motion. Shadowgraphic visualization of the convection pattern was used by Howle (1997a, b) to measure the wave pattern and use it as an input to a backstepping controller. A nonlinear feedback control strategy has been proposed by Or et al. (1999) for delaying the onset and stabilize long wavelength instabilities in the Marangoni-Bénard convection. The same configuration was studied by Bau (1999) who demonstrates analytically that, through the use of feedback control strategies, one can postpone the onset of motion. The case of a fluid layer subjected to an internal heating source, and cooled isothermally from above and below has been investigated by Marimbordes et al. (2002). Using a control strategy similar to that proposed by Tang and Bau (1993) it was demonstrated that, by controlling the heating power, the critical Rayleigh number for the onset of motion can be increased. Feedback control of the Marangoni-Bénard convection in a horizontal fluid layer with internal heat generation has been studied by Bachok and Arifin (2010). It was found that the critical Marangoni number decreases with the intensity of the internal heat generation. Also, with the feedback control, it was possible to increase the critical Marangoni number. The effect of control on the onset of thermal convection in a rectangular loop by changing its spatial orientation has been investigated by Bratsun et al. (2018). It was demonstrated theoretically and experimentally that the control method can successfully stabilize a no-motion state and time-dependent modes of convection. Recently, a few studies have also been concerned by the effect of feedback control on the onset of convection in micropolar fluids (Abidin et al. 2012; Mokhtar et al. 2012; Khalid et al. 2013; Mokhtar and Khalid 2016) and convection in a nanofluid (Mokhtar et al. 2017a, b; Khalid et al. 2017). Also, the use of imposed harmonic vibrations to control convection patterning and intensity in shallow cavities has been discussed by Lappa (2016).

The present paper investigates the effect of proportional and derivative controllers on the onset of convection in a fluid layer with uniform volumetric energy sources. The earliest study of the effect of non-linear temperature profile and boundary conditions on the onset of motion in a horizontal fluid layer is that of Sparrow et al. (1964). An experimental study was carried out by Tritton and Zarraga (1967) to investigate qualitatively the convection patterns produced by the instability of a horizontal layer of fluid with volumetric heat sources and cooled from above. The same problem was considered theoretically by Roberts (1967) and the critical Rayleigh number for the onset of motion was predicted on the basis of the linear stability theory. The stability of an infinite layer of fluid which loses heat throughout its volume at a constant rate has been considered by Watson (1968). It was found that the critical Rayleigh

number, for the onset of motion, decreases as the rate of heat loss increases. Linear and energy theory stability criteria have been used by Kulacki and Goldstein (1975) for fluid layers of infinite horizontal extent heated internally by a uniform volumetric energy source. The thermal coupling between the layer and its environment was modeled by a general mixed boundary condition in both the conduction state and the disturbance temperature. The critical Rayleigh numbers for the onset of motion were for various boundary conditions applied on the upper and lower boundaries.

More recently, the effect of internal heat generation on the onset of Bénard-Marangoni convection in a horizontal ferrofluid layer heated from below, in the presence of a vertical magnetic field, has been investigated by Nanjundappa et al. (2011). It is demonstrated that the combined effect of magnetic Rayleigh number and internal heat source is to hasten the onset of motion.

The paper is organized as follows. First, the physical model and mathematical formulation of the problem is presented. The linear stability theory is used in order to predict the critical Rayleigh number for the onset of motion as a function of controller gains. Then, some relevant details of the computational method utilized to solve the full governing equations are presented. Finally, the results from the numerical computations are discussed and conclusions are drawn.

Formulation of the Problem

The system under investigation is shown schematically in Fig. 1. A horizontal two-dimensional fluid layer of thickness L' is bounded by impermeable walls. A uniform internal heat generation per unit volume q' is applied on the layer by passing an electric current through a conducting fluid. The fluid has a constant dynamic viscosity μ and thermal conductivity k and assumed to be Newtonian and satisfy the Boussinesq approximation:

$$\rho = \rho_r[1 - \beta(T' - T_r')] \tag{1}$$

where ρ_r is the fluid density at temperature $T' = T_r'$ and β is the thermal expansion coefficient.

The governing equations are the usual Navier-Sokes equations and conservation of energy:

$$\nabla.\vec{V}' = 0 \tag{2}$$

$$\rho_r \frac{\partial \vec{V}'}{\partial t'} + \rho_r(\vec{V}'.\nabla)\vec{V}' = -\nabla P' + \mu\ \nabla^2\vec{V}' + \rho_r[1-\beta(T'-T_r')]\ \vec{g} \tag{3}$$

$$\frac{\partial T'}{\partial t'} + (\vec{V}'.\nabla)T' = \frac{k}{\rho_r C_p}\nabla^2 T' + \dot{q}' \tag{4}$$

where $\vec{V}'(u', v')$ is the velocity vector, P' the pressure, $\vec{g}$ the acceleration of gravity and C_p the specific heat of the fluid.

The boundary conditions for the velocity field are the no slip conditions on the horizontal walls of the system. Thermally, the layer is maintained at a constant temperature T_r'. Thus we have:

$$u' = v' = 0; \quad T' = T_r' \qquad \text{at } y' = 0, L' \tag{5}$$

The present Rayleigh-Bénard configuration is characterized by the fact that below a critical heating power the fluid is motionless and the vertical temperature distribution across the layer is the conductive one. Above this threshold a convective motion is generated which will modify the temperature distribution from its conductive distribution. The idea is to modulate the heat source $\dot{q}'$ in such a way to retard the onset of motion. In order to do so, an array of sensors located at position (x', y_s') detects the deviations of temperature $T'(x', y_s')$ from its conductive value $T_{cond}'(x', y_s')$. Then, an array of actuators modulates the intensity of the heat source $\dot{q}'(x')$ in proportion to the deviation in the corresponding fluid column, in order to suppress deviations from the rest state. Once the disturbances have been annihilated, the local controllers are turned off.

Thus, in Eq. 4, the specific heating power supplied to the fluid layer is expressed as:

$$\dot{q}' = (\dot{q}_E' + \dot{q}_A') \tag{6}$$

where the constant part of $\dot{q}'$ is given by $\dot{q}_E' = \sigma E'^2/\rho_r C_p$, σ is the electric conductivity and E' the electric field

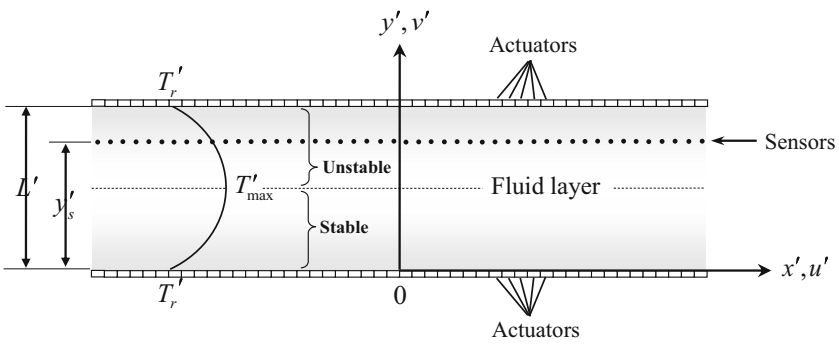

Fig. 1 Schematic diagram of the physical model and coordinate system

magnitude. The fluctuating part, $\dot{q}'_A(x')$, supplied to the system by the actuators follows the rule:

$$\dot{q}'_A(x',t') = -G'\,[T'(x',y'_s,t') - T'_{cond}(x',y'_s)] - G_t \frac{\partial T'(x',y'_s,t')}{\partial t'} \tag{7}$$

where G' and G_t are the proportional and derivative controllers gain, respectively.

The governing equations are nondimensionalized by scaling the length with L', time with L'^2/α, velocity with α/L', pressure with $\rho_r(\alpha/L')^2$ and the proportional controller coefficient (G') with α/L'^2. Also, we introduce the dimensionless temperature $T = (T' - T'_r)/(\dot{q}'_E L'^2/\alpha)$. Using these scales, Eqs. 2–4 can be transformed to the following dimensionless form:

$$\frac{\partial \Omega}{\partial t} + u\frac{\partial \Omega}{\partial x} + v\frac{\partial \Omega}{\partial y} = \mathrm{Pr}\,\nabla^2\Omega - \mathrm{Pr}\,Ra\frac{\partial T}{\partial x} \tag{8}$$

$$\frac{\partial T}{\partial t} + u\frac{\partial T}{\partial x} + v\frac{\partial T}{\partial y} = \nabla^2 T + \dot{q} \tag{9}$$

where $\Omega = -\nabla^2\Psi$ is the vorticity and Ψ is the usual stream function defined as $u = \partial\Psi/\partial y$ and $v = -\partial\Psi/\partial x$, such that the mass conservation is satisfied. $\mathrm{Pr} = \upsilon/\alpha$ is the Prandtl number, $Ra = g\beta'\dot{q}'_E L'^5/\upsilon\alpha^2$ is the Rayleigh number and υ the kinematic viscosity of the fluid.

The nondimensional heat source on the right hand side of Eq. 9 is given by

$$\dot{q}(x,t) = 1 - \dot{q}_A(x,t) \tag{10}$$

where:

$$\dot{q}_A(x,t) = G\,[T(x,y_s,t) - T_{cond}(x,y_s)] + G_t\frac{\partial T(x,y_s,t)}{\partial t} \tag{11}$$

Physically, the system cannot be cooled in its volume such that when $\dot{q}_A > 1$ the source term, Eq. 10, is set equal to zero.

The nondimensional boundary conditions at the walls of the layer are:

$$\Psi = \partial\Psi/\partial y = 0 \quad T = 0 \qquad \text{at } y = 0, 1 \tag{12}$$

When the fluid is motionless ($\Psi_{cond} = 0$), an equilibrium state is possible, provided that the Rayleigh number is below a critical value. For this situation, in the absence of a controller ($G = G_t = 0$), Eqs. 8–9 yield the following temperature profile for the conductive state:

$$T_{cond} = (y - y^2)/2 \tag{13}$$

The above temperature profile is parabolic with the maximum at the center. Thus, the lower part of the layer is stable and the upper one unstable (see Fig. 1). This situation is similar to the case of a layer of cold water in the neighborhood of 4 °C, point at which the density of water reaches a maximum value (see for instance Mamou et al. 1999).

Linear Stability Analysis

In this section the onset of motion is investigated on the basis of the linear stability theory. To do so, the stability to small perturbations from the quiescent state (Ψ_{cond}, T_{cond}) is examined now. It is convenient to rewrite the governing equations using $\psi = \Psi - \Psi_{cond}$ and $\theta = T - T_{cond}$. As usual, the perturbed solution is assumed to have the following functional form:

$$\left.\begin{aligned}\psi(t,x,y) &= \tilde{\psi}(y)e^{pt+iax}\\ \theta(t,x,y) &= \tilde{\theta}(y)e^{pt+iax}\end{aligned}\right\} \tag{14}$$

where $\tilde{\psi}(y)$ and $\tilde{\theta}(y)$ describe the vertical perturbation profiles and $p = p_r + i\omega$ is the complex growth rate of the perturbation. In the above equation $a = 2\pi/\lambda$ is the real wave number, λ the wavelength, p_r the grow rate of instability and ω the frequency of instability.

Introducing Eq. 14 into Eqs. 8 and 9 and neglecting second higher-order nonlinear terms yields the following linear system:

$$\mathrm{Pr}[(D^2 - a^2)(D^2 - a^2)\tilde{\psi} - iaRa\tilde{\theta}] = p(D^2 - a^2)\tilde{\psi} \tag{15}$$

$$(D^2 - a^2)\tilde{\theta} + ia\tilde{\psi}DT_{cond} - G\tilde{\theta}(y_s) = p[\tilde{\theta} + G_t\tilde{\theta}(y_s)] \tag{16}$$

The boundary conditions, corresponding to Eq. 11 are:

$$\tilde{\psi} = D\tilde{\psi} = 0; \qquad \tilde{\theta} = 0 \text{ at } y = 0, \tag{17}$$

where $D = d/dy$.

The perturbed state Eqs. 15–16 with the boundary conditions (17) may be written in a compact matrix form as:

$$M_A(a)Y = pM_B(a)Y \tag{18}$$

where $Y = [\tilde{\psi}, \tilde{\theta}]$ is a two-component vector of the perturbation and $M_A(a)$ and $M_B(a)$ are two linear differential operators that depend on the control parameters Ra, Pr, y_s, G and G_t.

The set of Eqs. 18 is solved using a finite differences scheme. The system is discretized using a fourth-order scheme in the domain between $y = 0$ and $y = 1$. For N computational points, the resulting discrete system has 2N eigenvalues (corresponding to variables $\tilde{\psi}$ and $\tilde{\theta}$, respectively) that can be found using a standard IMSL subroutine such as DGVCCG. The value of Ra for which the maximal growth rate p_r among the 2N eigenvalues cancels is determined iteratively by Newton's method (for details on the procedure see for instance Weerakoon 1996), holding a, Pr, y_s, G and G_t constant.

Table 1 Comparison between the present numerical solution of the linear stability analysis and the results of Kulacki and Goldstein (1975)

Present N=100		Present N=150		Present N=200		Kulacki and Goldstein (1975)	
Ra_c	a_c	Ra_c	a_c	Ra_c	a_c	Ra_c	a_c
37317.76	4.00	37321.90	4.00	37323.34	4.00	37324.80	4.00

The validation of the numerical code has been performed for the case of an uncontrolled system. The precision of the value of the critical Rayleigh number and wave number predicted by the present numerical procedure depends on the grid number N. Numerical tests, using various mesh size were done for the same conditions in order to determine the best compromise between accuracy of the results and computing time. Typical results are presented in Table 1 which shows that for N≥100 the present study is found to agree very well with the results reported in the past by Kulacki and Goldstein (1975). Based on these results, the value N = 150 was adopted for this study. For the case of a controlled system the code was compared with the results obtained in the past by Tang (1996) (Table 2). A good agreement is also obtained, the maximum deviation been of the order of 0.6%.

Numerical Solution

The solution of the governing Eqs. 8–11 and boundary conditions (12) is obtained using a finite difference method with uniform grid size. The energy equation was solved using the alternating direction implicit method (ADI). The stream function field was solved using over relaxation method (SOR) and know temperature distribution. A first order backward finite difference scheme is employed to discretize the temporal terms appearing in the governing equations. A line-by-line tridiagonal matrix algorithm with relaxation is used in conjunction with iterations to solve the nonlinear discretized equations. We consider that convergence is reached when $\sum_i \sum_j (b_{ij}^{new} - b_{ij}^{old}) / \sum_i \sum_j b_{ij}^{new} \leq 10^{-6}$ is satisfied, where b stands for Ψ, Ω and T. The subscripts i and j denote grid locations in the (x, y) plane while superscripts new and old refer to values evaluated at time steps $t + \Delta t$ and t, respectively. A further decrease of the convergence criteria 10^{-6} does not cause any significant change in the final results.

Numerical tests, using various mesh sizes, were done for the same conditions in order to determine the best compromise between accuracy of the results and computer time. Typical results in terms of average Nusselt number are presented in Table 3 for the case $Ra = 10^5$, Pr = 7, $G = 0$ and $A = 10$, in which A is the aspect ratio (length/height) of the rectangular domain considered in the numerical procedure. Based on this accuracy test, most of the calculations presented in this paper were performed using a 40×372 grid.

Table 4 shows a comparison between the prediction of the linear stability theory and the numerical solution of the full governing equations for Pr = 7, $y_s = 0.77$ and various values of G. As discussed above, for an uncontrolled layer ($G = 0$), the linear stability theory predicts that the onset of steady state motion ($\omega_c = 0$) occurs at a critical Rayleigh number $Ra_c = 37323$. This result was verified numerically by considering a unicellular flow confined in a cavity with free vertical boundaries. First, a result was obtained for a Rayleigh number slightly above the critical value predicted by the linear stability theory. Then, the Rayleigh number was decreased step by step, using the previous results as initial conditions in the numerical code, until the rest state was reached. In this way it was found that, $Ra_c = 37500$, which is close (within 0.5%) to the prediction of the linear stability theory. Similarly, for a controlled layer ($G \neq 0$), the agreement between the two methods is observed to be excellent for both steady ($\omega_c = 0$) and unsteady ($\omega_c \neq 0$) onsets of motion. It is worthwhile to mention that, using a commercial code, a few numerical results concerning this problem have been reported by Marimbordes et al. (2002). However, these authors have not tried to compare these results with those of their linear stability model for the controlled system ($G \neq 0$).

Table 2 Validation of the numerical code for a controlled system and for Pr = 0.7 (r = Ra_c/1708)

	G = 0		G = 2		G = 3	
	r	a_c	r	a_c	r	a_c
Tang (1996)	1	3.117	1.66	3.653	2.07	3.877
Present	1	3.116	1.65	3.649	2.06	3.870

Table 3 Accuracy test for $Ra = 10^5$, Pr = 7, $A = 10$ and $G = 0$

	Nodes			
	20×266	30×266	40×372	50×372
Nu_m	4.775	4.737	4.722	4.714

Table 4 Comparison between the results of the linear stability theory and the results of numerical simulation for Pr = 7 and $y_s = 0.77$

	Linear stability theory		Numerical simulation	
G	Ra_c	ω_c	Ra_c	ω_c
0	37323	0	37500	0
30	104119	0	104500	0
65	211816	42.9	213000	41.9
90	229296	90.3	230000	89.5

Result and Discussion

The present problem is governed by five parameters, namely Ra, Pr, G, G_t and y_s. Most of the results presented in this study were obtained for the particular case Pr = 7 such that the value of the Prandtl number will be specified in the text only when it is different from this value. First, the results obtained a proportional controller is discussed. Then, the effect of a derivative controller is investigated.

Proportional Controller

In the section, the case of the proportional controller ($G \neq 0, G_t = 0$) is considered. This situation has been investigated in the past by Marimbordes et al. (2002). However, the linear stability theory developed by the authors relies on the assumption that the exchange of stability can be assumed. This is not always true as it will be demonstrated here. Also, as discussed above, they only retained the two first steady modes in the Fourier series used to analyze the stability of the conductive state. It is found in the present study that, under certain conditions, more modes are necessary to obtain accurate results. Using linear stability analysis and numerical solutions of the full governing equations it will be demonstrated in this section that one can postpone (prepone) considerably the transition from the no-motion conductive state to the motion one (steady or unsteady). Also, it will be shown that both the critical Rayleigh numbers for the onset of steady and unsteady motions depend strongly upon the magnitude of the heating power G and vertical position of the temperature sensor y_s. The theoretical maximum and minimum critical Rayleigh numbers possible for the present system are predicted in terms of both G and y_s.

Figure 2a and b depicts the marginal stability curves obtained numerically, in terms of the critical Rayleigh number at the onset of motion, Ra, versus the wave number, a. The results presented in Fig. 2a were obtained for various values of the controller gain, G, when the temperature sensors are located at position $y_s = 0.75$. For a given curve, it is seen that the critical Rayleigh number $Ra \to \infty$ as $a \to 0$. Upon increasing a, the critical Rayleigh number decreases quickly, reaches a minimum at a given critical wave number, and then starts to increase again. The global minimum yields the critical Rayleigh number Ra_c and the corresponding critical wave number a_c. For an uncontrolled system ($G = 0$), it is found that, $Ra_c = 37323$ at $a_c = 4$, in agreement with the numerical results obtained in the past by Kulacki and Goldstein (1975). A bird eye view on the graph shows that the feedback control ($G > 0$) has a stabilizing effect on the system such that Ra_c increases with an increase of G. Also, it is observed that the loss of stability occurs at larger wave numbers, i.e. shorter wavelengths. The solid lines in the graph correspond to a supercritical bifurcation occurring through a real eigenvalue and exchange of stability. On the other hand, the dashed lines indicate a Hopf's bifurcation, for which the onset of motion is time-dependent and the eigenvalue imaginary.

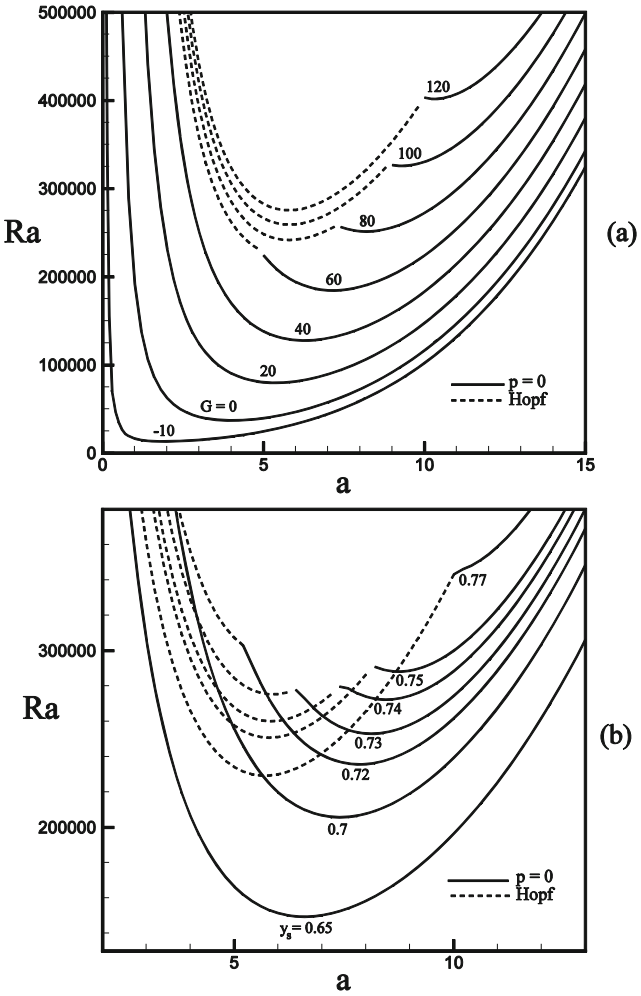

Fig. 2 The Rayleigh number Ra at the onset of convection as a function of the wave number a: **a** effect of the controller gain G, $y_s = 0.75$; **b** effect of the position of the temperature sensors y_s, $G = 90$

For $G \leq 40$, the loss of stability occurs through a real eigenvalue. However for higher values of G the marginal stability curves exhibit two minima, one corresponding to a real eigenvalue and the second to an imaginary one. The critical Rayleigh numbers, corresponding to these two eigenvalues, are approximately equal for $G \approx 76.3$ (not presented in the graph). For this situation a bistability phenomenon is observed and the two modes of convection are possible simultaneously. For higher (lower) values of G, the minimum corresponding to an Hopf's (supercritical) bifurcation becomes the global critical Rayleigh number. Also presented in the graph is the result obtained for a negative value of the controller gain, namely $G = -10$. A negative value of G implies that the actuators amplify the deviations of the probe temperature sensors from their conductive values. As a result, the system is now destabilized and the onset of motion occurs at a critical Rayleigh number lower than the value corresponding to uncontrolled situation. The effect of the position of the temperature sensors, y_s, on the marginal stability curves is depicted in Fig. 2b for $G = 90$. The results indicate that y_s has a considerable influence on the onset of convection through both real and imaginary eigenvalues. This point will be discussed in details below.

In the case of a classical Rayleigh-Bénard problem, i.e. an unstable horizontal layer of fluid heated from below and cooled from above, it has been demonstrated by Tang and Bau (1995) that the position y_s of the temperature sensors affects the value of the corresponding critical Rayleigh number Ra_c, for the onset of motion of the controlled system. In the present problem we are dealing with a more complicated system, namely a potentially unstable layer of fluid topping a stable one (see Fig. 1). It is thus expected that, depending in which of these two layers the sensors are positioned, the results will be quite different. This point is illustrated in Fig. 3a–c which shows the critical Rayleigh number Ra_c, wave number a_c and frequency ω_c, at the onset of convection, as a function of the vertical position of the temperature sensors y_s for various values of G. Here also, the solid lines correspond to a bifurcation from the rest state into a steady flow while the dashed lines represent bifurcation into a time-periodic flow. In the absence of a controller ($G = 0$), the classical situation is recovered for which $Ra_c = 37323$, $a_c = 4$ and $\omega_c = 0$. Upon applying a feedback gain of $G = 30$ it is seen that, depending upon the position of the temperature probe y_s, the control loop stabilizes ($Ra_c > 37323$) or destabilizes ($Ra_c < 37323$) the system. In order to understand this behaviour, Fig. 4a–c shows the set of flow (left) and temperature fields (right) predicted by the linear stability theory, as they exist at incipient convection, for $G = 30$ and $y_s = 0.77$, 0.4 and 0.22 respectively. All these flow and temperature patterns are represented over one wavelength. According to Fig. 3a,

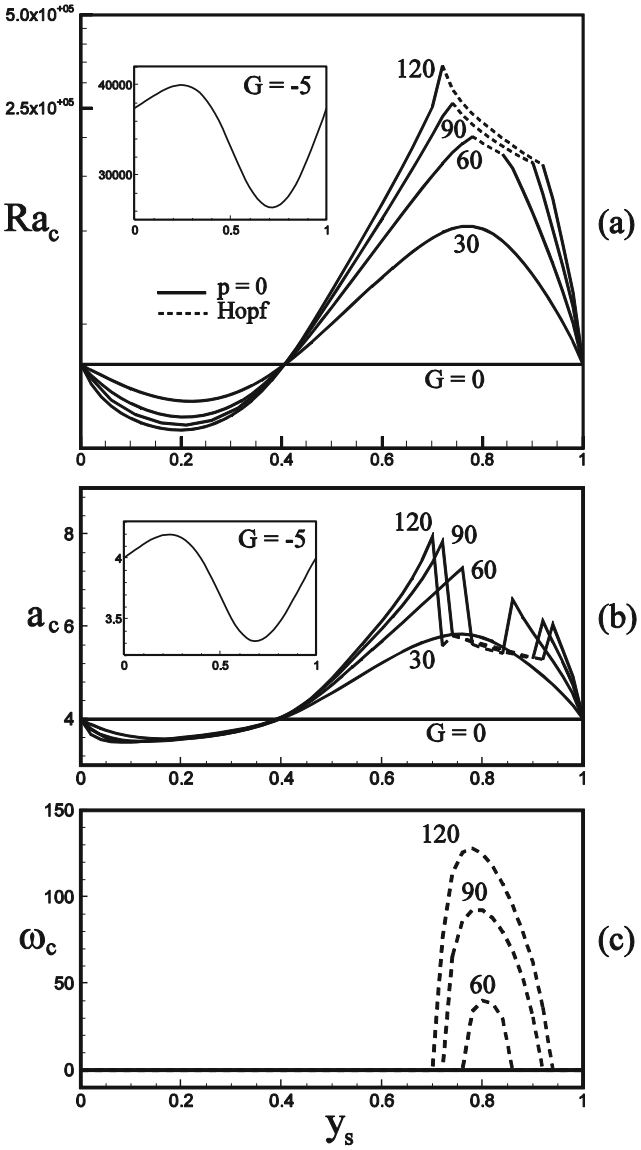

Fig. 3 The effect of the positions of the temperature sensors y_s and controller gain G on **a** critical Rayleigh number Ra_c; **b** wave number a_c; **c** frequency ω_c

for $G = 30$, the maximum stabilization of the layer occurs for $y_s = 0.77$. For this situation it is observed from Fig. 4a that the induced convection flow pattern consists in a pair counter rotating cells in the upper part (unstable) of the layer. This induced convective motion is not limited to the thickness of the unstable layer ($1/2 \leq y \leq 1$) but penetrates considerably inside the stable one ($0 \leq y \leq 1/2$). Furthermore, this flow pattern gives rise, trough viscous forces, to a weak circulation at the bottom of the layer. The distribution of the stream function deviations from the rest state, $\psi(y)$ through the center of the upper clockwise circulation, with respect to the vertical position y, is depicted for information. The corresponding vertical distribution of temperature perturbations, $\theta(y)$, are also

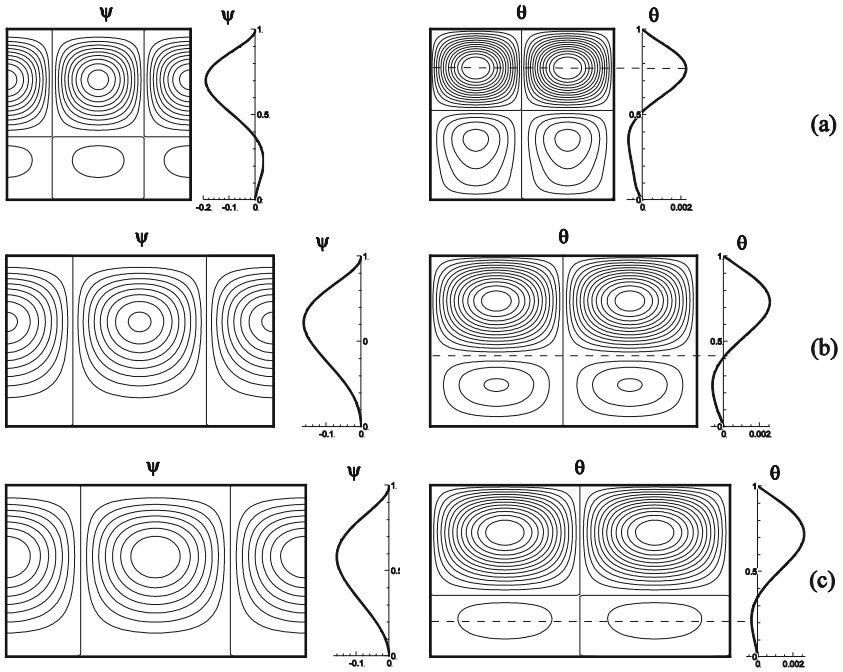

Fig. 4 Incipient flow patterns (left) and temperature perturbation (right) fields for $G = 30$ for various positions of the temperature sensor: **a** $y_s = 0.77$; **b** $y_s = 0, 0.4, 1$; **c** $y_s = 0.22$

illustrated in the graph. It is clear that, in the upper part of the system, the maximum temperature perturbation $\theta(y)$, occurs at $y_s = 0.77$, position at which the temperature sensor yields an optimum stabilization of the system. When the sensor is moved at $y_s = 0.4$, Fig. 3a indicates that the uncontrolled system is recovered. For this particular value of y_s it is seen from Fig. 4b that the temperature fluctuation is nil, $(\theta(y_s = 0.44) = 0)$. Thus, the controller does not have any effect on the perturbations. Naturally, a similar behaviour occurs when the sensor is moved to the top or the bottom of the fluid layer where the temperature fluctuations are also nil. This explains why, at $y_s = 0$, 0.4 and 1, the critical Rayleigh number of the uncontrolled classical situation is recovered. One interesting point illustrated by Fig. 3a is the fact that when the sensor is moved below $y_s = 0.4$ the controller now destabilizes the layer such that convection occurs at Rayleigh numbers below the classical value $Ra_c = 37323$. This behaviour follows from the fact that in the region $0 \leq y_s \leq 0.4$, at a given value y_s, the temperature fluctuations are colder than his environment, giving rise to an descendant fluid motion. To maintain the no-motion state the controller increases slightly the power input that must be supplied to this fluid column. Consequently, the temperature fluctuations in the upper part of the layer $y_s \geq 0.4$ are promoted. In this way, the controller enhances the strength of the buoyancy forces in the unstable part of the fluid layer such that the system is destabilized earlier. The resulting critical Rayleigh number of the controlled system is thus now significantly lower than for the uncontrolled one. It is also seen from Fig. 3a that the minimum Rayleigh number, namely Ra_c =28350 occurs at $y_s = 0.22$. This position corresponds, according to Fig. 4c, to the maximum temperature fluctuation in the bottom of the layer. Also illustrated in Fig. 3a is the result obtained for $G = -5$, i.e. upon changing the sign in front of the heat source. As expected, for this situation the control loop stabilizes (destabilizes) the system when $y_s \leq 0.38$ $(y_s \geq 0.38)$.

Figure 5a–c depicts the critical Rayleigh number, Ra_c, wave number a_c and frequency ω_c, at the onset of motion, as a function of the control gain G for various values of y_s. When the temperature sensors are positioned at $y_s = 0.6$and 0.7 it is observed that upon increasing G the value of Ra_c increases from $Ra_c = 37325$ at $G = 0$ to reach asymptotically the limit $Ra_c \to 2.1 \times 10^5$ (5.1×10^5), as the value G is made sufficiently large. The corresponding variation of the critical wave number is from $a_c = 4$ to $a_c \to 6.8(8.8)$. It is noted that the frequency ω_c is identically zero since, for these positions of the temperature sensors, the loss of stability occurs through exchange of stability, independently of the value of G. Upon moving the temperature sensors at the positions $y_s = 0.75$, 0.80 and 0.90, the resulting curves are seen to be quite different. Thus, for relatively small values of G, the principle of exchange of stability prevails and the onset of convection is steady (solid lines). However, the results indicate that for a higher value of G, which depends upon y_s, the loss of stability occurs into a time dependent motion (dashed lines). Figure 5b and c indicate that the corresponding wavenumber decreases while the frequency ω_C increases significantly. As the value of G is increased further, a limit is reached such that Ra_C remains constant. The loss

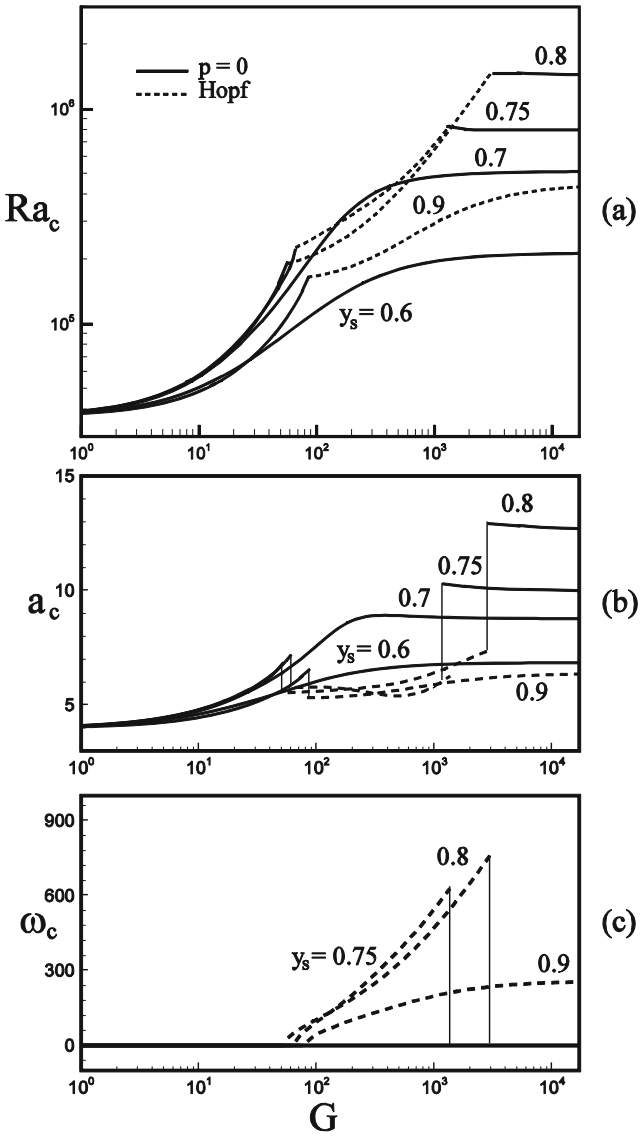

Fig. 5 Effect of controller's gain G on **a** critical Rayleigh number Ra_c; **b** wave number a_c; **c** frequency ω_c for $y_s = 0.6, 0.7, 0.75, 0.8$ and 0.9

of stability becomes again steady (excepted for the case $y_s = 0.9$). It is noted that the evolution of Ra_c with G has been investigated by Marimbordes et al. (2002) for four different values of y_s. It was found that, independently of the value of G, the position $y_s = 0.75$ was the more effective place to place the temperature probe. It was explained that this is probably due to the fact that this position corresponds to the center of the cellular structures. This is not always true since the convective cells in the upper part of the layer can penetrate inside the lower stable layer (see Fig. 4). Furthermore, as demonstrated here, the optimal position of the thermal probes relies on the temperature perturbation profiles predicted by the linear stability analysis. For large values of G, it has not be possible to reproduce the results reported by Marimbordes et al. (2002).

The critical Rayleigh number Ra_c, wave number a_c and frequency ω_c, versus the Prandtl number Pr, are displayed in Fig. 6a for $y_s = 0.8$ and $G = 200$. For this situation, Fig. 5 indicates that the onset of motion is time dependent. The results show that there is a minimum value $Ra_c = 2.6 \times 10^5$ at Pr = 4.93, for which $a_c = 5.66$ and $\omega_c = 171.5$. Upon decreasing the Prandtl number below this value it is seen that the critical Rayleigh number first increases sharply to reach asymptotically the value $Ra_c = 6.7 \times 10^5$. The wavelength is also observed to increase until it reaches a plateau while the frequency decreases monotonously. This behavior is due to the fact that a decrease of the Prandlt number corresponds to an increase of the thermal diffusivity α. As a result, the thermal perturbations responsible for the destabilization of the base temperature profile are dissipated faster as α(Pr) increases (decreases). For information, the critical perturbations for the stream function ψ and temperature θ fields, are presented in Fig. 6c and d for Prandtl numbers of Pr = 10^{-3}, 4.94 and 10^3, respectively.

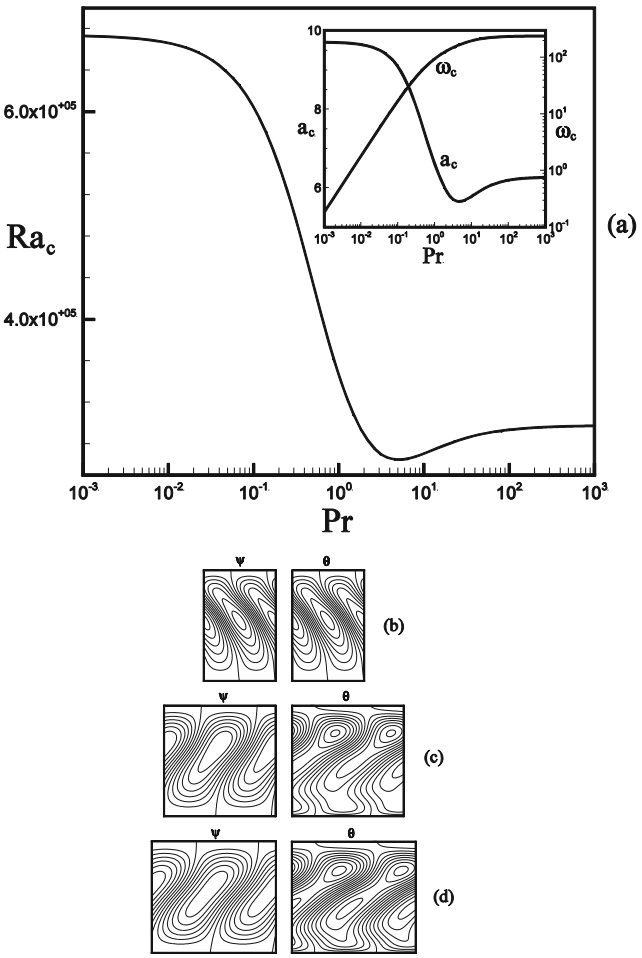

Fig. 6 **a** Effect of Prandtl number Pr on critical Rayleigh number Ra_c, wavenumber a_c and frequency ω_c for $G = 200$ and $y_s = 0.8$. Critical perturbations solutions ψ and θ at **b** Pr = 10^{-3}, **c** Pr = 4.94 and **d** Pr = 10^3, respectively

Figure 7a shows the maximum (minimum) values of the normalized critical Rayleigh numbers $r_{\max}(r_{\min})$, as function of the controllers gain G. The parameter r is defined as the ratio between the critical Rayleigh number Ra_c of the controlled layer and that of the uncontrolled one ($Ra_c = 37323$). The graph indicates that for approximately $G \leq 1$ the actuators are inoperative such that $r_{\max} = r_{\min} \approx 1$. As the value of the controller gain is made larger, $1 \leq G \leq 10^2$, it is seen that $r_{\max}$ increases sharply up to $r_{\max} \approx 9$, while $r_{\min}$ decreases down to $r_{\min} \approx 0.60$. The positions of the thermal sensors $y_{s\,\max}$ ($y_{s\,\min}$), required to stabilize (destabilize) in such a way the system are depicted in Fig. 7b.

Figure 8 illustrates the maximum (minimum) value of the stream function, $\Psi_{\max}(\Psi_{\min})$, predicted by the numerical solution of the full governing equations, as a function of time t for $y_s = 0.77$. For a control gain $G = 30$ and $Ra = 1.05 \times 10^5$, i.e. slightly above the critical Rayleigh number $Ra_c = 1.04 \times 10^5$ predicted by the linear stability theory (Table 4), Fig. 8a indicates that the system remains stable up to $t \approx 21.3$. Above this value a steady flow pattern, consisting of two superposed counterrotating cells, occurs. This situation persists up to $t = 24$, at which the intensity of the controller gain is increased up to $G = 40$. Almost instantaneously, the controller suppresses the fully established motion and the rest state is restored (see the isotherm patterns at $t = 24$ and 26, respectively). Figure 8b shows similar results obtained for $G = 65$ and $Ra = 2.17 \times 10^5$, for which according to Table 4 a Hopf's bifurcation occurs at the onset of motion ($Ra_c = 2.12 \times 10^5$). The numerical results indicate that this is indeed the case since, above approximately $t \approx 15.7$, a permanently oscillating flow regime is observed. However, at time $t \approx 21.5$, the results show that the system bifurcates toward a steady bi-cellular flow pattern. At time $t = 24$, upon increasing the magnitude of the controller gain up to $G = 90$ the convective motion is inhibited and quickly reaches a steady state, after a short oscillating regime.

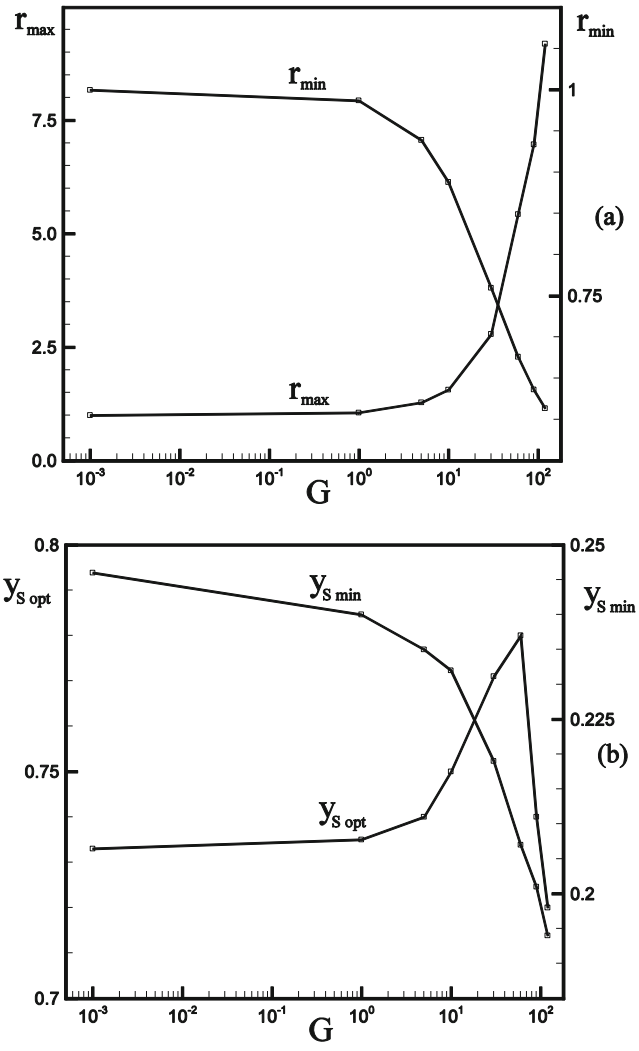

Fig. 7 Effect of the proportional gain of control G; **a** position of the temperature sensors $y_{sopt}(y_{s\,\min})$ for a maximum (minimum) critical Rayleigh number Ra_c; **b** reduced critical Rayleigh number r

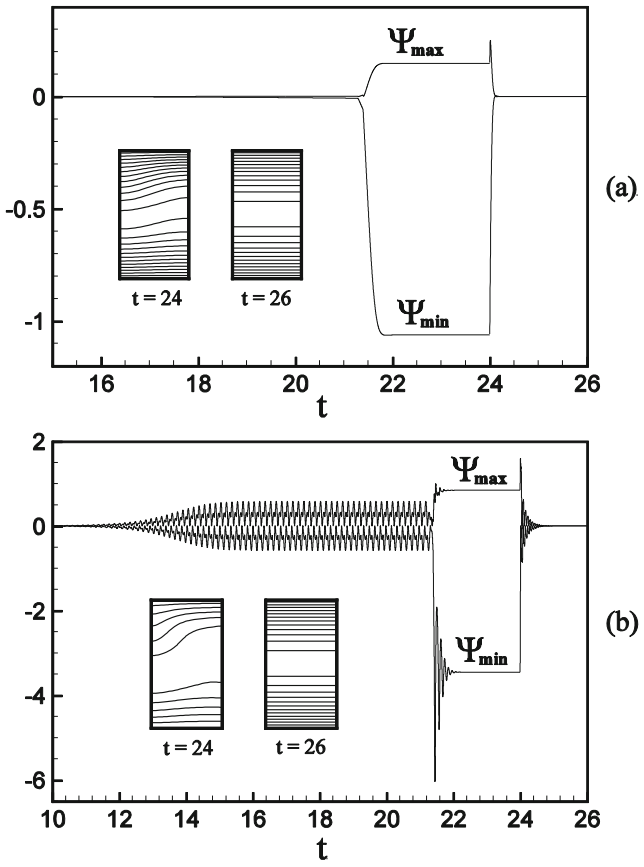

Fig. 8 Time evolution of $\Psi_{\max}$ and $\Psi_{\min}$ for $y_s = 0.77$; **a** $Ra = 1.05 \times 10^5$, $G = 30$; **b** $Ra = 2.17 \times 10^5$, $G = 65$

Derivative Controller

In this section the effect of applying both proportional and derivative controllers ($G \neq 0, G_t \neq 0$), on the onset of motion of the system, is investigated. Based on the linear stability theory it will be shown that, upon keeping constant the proportional controller, the use of a derivative strategy postpones the onset of motion of the system. Here again the critical Rayleigh number depends upon the heating power G_t and vertical position of the temperature sensor y_s. Also, numerical solutions of the full governing equations illustrate the fact that upon applying a derivative controller gain on an initially periodically oscillating flow regime the rest state is restored.

Figure 9 depicts the influence of the differential controller's gain G_t on the marginal stability curve, namely the Rayleigh number Ra versus the wave number a at the onset of motion, for $G = 100$ and $y_s = 0.75$. Here again the solid lines correspond to steady flows (exchange of stability) and dashed one to oscillating flows (Hopf 's bifurcation). In the absence of a differential controller ($G_t = 0$) the loss of stability occurs into a time dependent motion, as also indicated by Fig. 5. The critical Rayleigh number for this situation is given by $Ra_c = 2.6 \times 10^5$ and the corresponding wave number is $a_c = 5.8$. Upon increasing the value of G_t it is observed that both the convection threshold Ra_c and wave number a_c are promoted. However, as can be seen by the graph in the small window included in Fig. 9, for $G_t \approx 0.24$ the value of the critical Rayleigh number reaches a constant value $Ra_c = 3.3 \times 10^5$. Naturally, there is no point to increase the value of the differential controller's gain above this value of G_t since no further increases in the critical Rayleigh number is possible.

The effect of the position of the temperature sensors y_s and controller's gain G_t on the critical Rayleigh number Ra_c is illustrated in Fig. 10 for $G = 400$. When the strength of the differential controller is sufficiently weak, according to the linear stability theory, the onset of motion occurs into an oscillatory motion for all the values of y_s considered here. For $y_s = 0.75$ it is seen that, upon increasing the value of the differential controller up to $G_t \approx 0.6$, the critical Rayleigh number increases from $Ra_c = 4.2 \times 10^5$ to a maximum value $Ra_c = 8.1 \times 10^5$ at which the flow is stable as indicated by the horizontal solid line. Here again, there is no point to increase the value of the differential controller higher than $G_t \approx 0.6$ since no gain in the critical Rayleigh number can be obtained. The results obtained for $y_s = 0.76$ are similar, excepted that upon increasing the value of G_t, it is observed that the horizontal plateau corresponding to a steady flow is maintained only up to $G_t \approx 22.5$. Above this value, the flow becomes oscillatory again and the value of Ra_c decreases slightly. Finally, when $y_s = 0.8$ the onset of motion occurs always through Hopf's bifurcations, independently of the value of G_t. Also depicted in the graph is the evolution of Ra versus a for $y_s = 0.8$ and $G_t = 3$.

Figure 11a shows the evolution of the maximum (minimum) value of the stream function, $\Psi_{\max}(\Psi_{\min})$, predicted by the numerical solution of the full governing equations, as a function of time t for $G = 100$ and $y_s = 0.75$. For this situation, according to the linear stability theory, it is found that $Ra_c = 256306$, $a_c = 5.79$ and $\omega_c = 94.3$ for $G_t = 0$. The numerical results presented here were

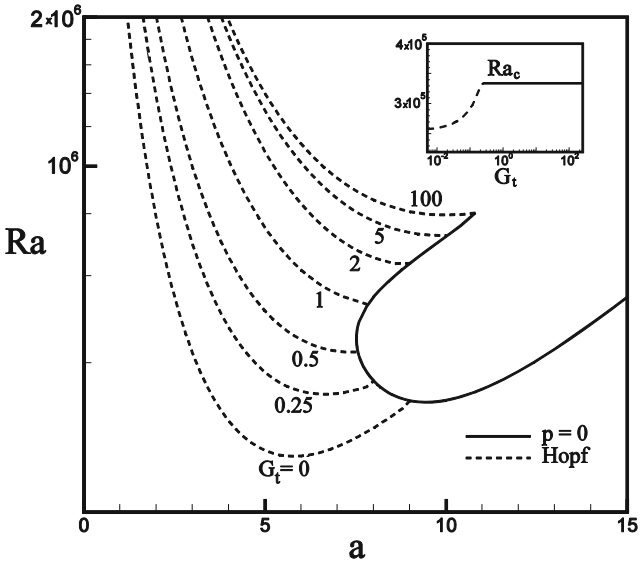

Fig. 9 The Rayleigh number Ra at the onset of convection as a function of the wave number, a and differential controller's gain G_t for $G = 100$ and $y_s = 0.75$

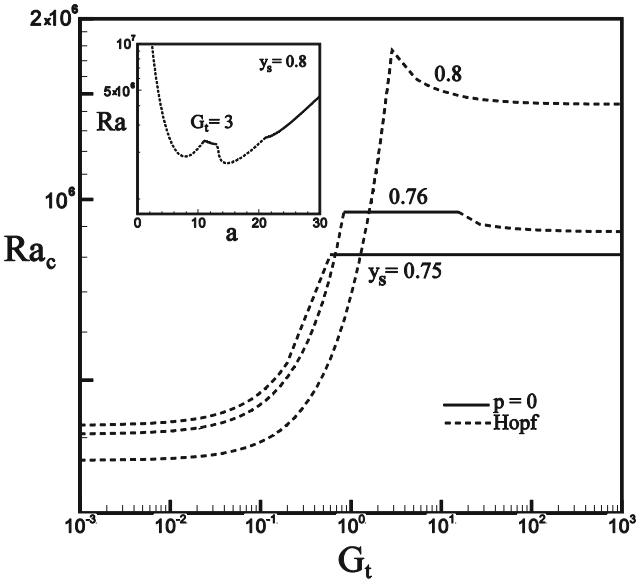

Fig. 10 The effect of the position y_s of the temperature sensors and differential controller's gain G_t on the critical Rayleigh number Ra_c for $G = 400$

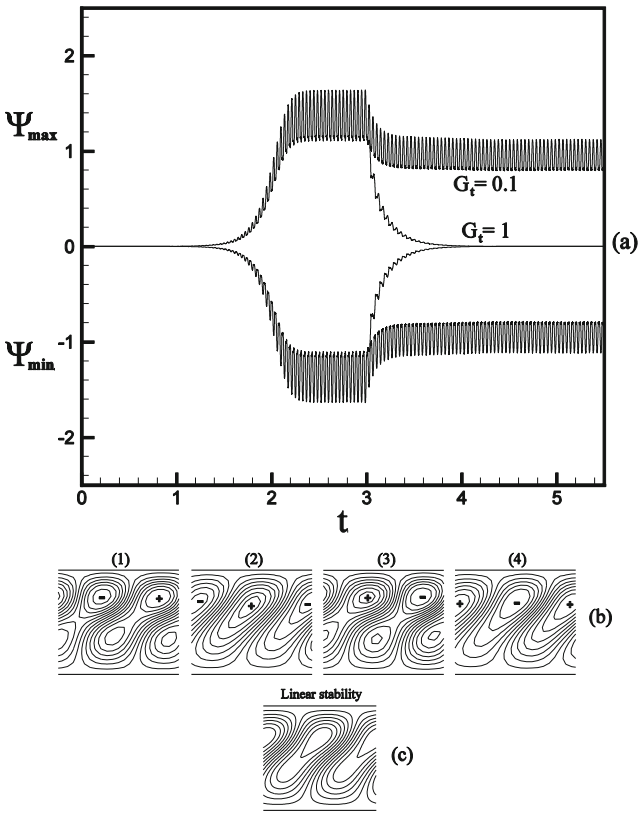

Fig. 11 **a** Time evolution of Ψ_{max} and Ψ_{min} for $Ra = 3 \times 10^5$, $y_s = 0.75$, $G = 100$, and $G_t = 0$, 0.1 and 1; **b** time history flow patterns obtained numerically for $G_t = 0$ at given values of time t during one cycle; **c** flow pattern predicted by the linear stability theory at time $t = 0$

obtained by considering a rectangular domain of aspect ratio (length / height) $A = 10.9$. This value corresponds to ten times the wave number predicted by the linear stability in the absence of controller gain, i.e. for $G_t = 0$. Thus, upon starting the numerical results with the rest state and pure conduction as initial conditions, it is seen that the flow is unsteady, as predicted by the linear stability theory. It is observed that, above approximately $t \geq 2.2$, a periodically oscillating flow regime is reached. The flow patterns (1)-(4) obtained numerically at various time t during a cycle is illustrated in Fig. 11b. The results indicate that the flow, at time (1), is bicellular with a large counterclockwise cell in the center of the computing domain. As the time is increased the flow pattern starts to restructure, such that at time (4) a large clockwise circulating cell occupies now the center of the computing domain. The flow pattern predicted by the linear stability theory is presented in Fig. 11c and is seen to be qualitatively in good agreement with the numerical predictions of the full governing equations. The effect of the combined action of the proportional and derivative controllers is illustrated in Fig. 11a. At time $t = 3$, upon applying a relatively small controller's gain $G_t = 0.1$, the numerical solution shows that the flow patterns remains oscillatory even though if the strength of the convective flow is reduced. However, upon increasing the controller' gain up to $G_t = 1$, the results indicate that the rest state is restored.

Conclusion

In this paper we have investigated the effect of a controller to postpone (or advance) the onset of motion in a horizontal fluid layer confined between two isothermal plates and subjected to internal heat generation. The present problem is characterized by a vertical parabolic temperature profile such that the upper half of the fluid layer is unstable while the lower one is stable. The governing parameters of the problem are the Rayleigh number, Ra, Prandtl number, Pr, position of the temperature sensors, y_s, the proportional controller's gain, G and the derivative controller's gain, G_t. The linear stability theory is used to predict the instability threshold for the controlled system. A numerical study of convective motion in the fluid layer is also performed, using a finite differences method. The main findings of the present study can be summarized as follows:

1° Based on the linear stability theory it has been demonstrated that, for the system considered here, the onset of Rayleigh-Bénard convection can be significantly affected by a proportional controller.
2° The position of the temperature sensors has been found to be important. Thus, within the unstable layer, there is an optimal position $y_{s\,\max}$ at which the loss of stability occurs at significantly higher Rayleigh numbers ($r_{\max} \approx 9$) than in the uncontrolled case. However, within the stable layer, the effect of the temperature sensors is to advance the onset of motion. The advance in the onset of motion is maximum ($r_{\min} \approx 0.60$) at a given position $y_{s\,\min}$.
3° The linear stability theory indicates that, depending on the controlling parameters of the problem, the onset of motion is not always steady but can be time-dependent (Hopf's bifurcation). This type of convection can be suppressed with a derivative controller.

The results of the linear stability theory have been confirmed by a numerical solution of the full governing equations.

References

Abidin, N.H.Z., Mokhtar, N.F.M., Arbin, N., Said, J.M., Arifin, N.M.: Marangoni convection in a micropolar fluid with feedback control. In: IEEE Symposium on Business and Industrial Applications, pp. 558–562 (2012)

Bachok, N., Arifin, N.M.D.: Feedback control of the Marangoni-Bénard convection in a horizontal fluid layer with internal heat generation. Microgravity Sci. Technol **22**, 97–105 (2010)
Bau, H.H.: Control of Marangoni-Bénard convection. Int. J. Heat Mass Transfer. **42**, 1327–1341 (1999)
Bénard, H.: Les tourbillons cellulaires dans une nappe liquide. Rev. Gén. Sci. Pures Appl. **11**, 1261–1271 (1900)
Bratsun, D., Krasnyakov, I., Zyuzgin, A.: Active control of thermal convection in a rectangular loop by changing its spatial orientation. Microgravity Sci. Technol. **30**, 43–52 (2018)
Chandrasekhar, S.: Hydrodynamic and hydromagnetic stability. Courier Dover, New York (1961)
Delucas, L.J., Moore, K.M., Long, M.L., Rouleau, R., Bray, T., Crysel, W., Weise, L.: Protein crystal growth in space, past and future. J. Crystal Growth **237-239**, 1646–1650 (2002)
Getling, A.V.: Rayleigh-Bénard convection: Structures and dynamics. World Scientific, Singapore (1998)
Howle, L.E.: Active control of Rayleigh-Bénard convection. Phys. Fluids **9**, 1861–1863 (1997a)
Howle, L.E.: Control of Rayleigh-Bénard convection in a small aspect ratio container. Int. J. Heat Mass Trans **40**, 817–822 (1997b)
Khalid, I.K., Mokhtar, N.F.M., Arifin, N.M.: Rayleigh-Bénard convection in microplar fluid with feedback control effect. World Appl. Sci. J. **21**, 112–118 (2013)
Khalid, I.K., Mokhtar, N.F.M., Hashim, I., Ibrahim, Z.B., Gani, S.S.A.: Effect of internal heat source on the onset of double-diffusive convection in a rotating nanofluid layer with feedback control strategy. Advances in Mathematical Physics, 2789024 (2017)
Kulacki, F.A., Goldstein, R.J.: Hydrodynamic instability in fluid layers with uniform volumetric energy sources. Appl. Sci. Res. **31**, 81–109 (1975)
Lappa, M.: Control of convection patterning and intensity in shallow cavities by harmonic vibrations. Microgravity Sci. Technol. **28**, 29–39 (2016)
Maekawa, T., Tanasawa, I.: Effect of magnetic field on onset of Marangoni convection. Int. J. Heat Mass Transfer **31**, 285–293 (1988)
Mamou, M., Robillard, L., Vasseur, P.: Thermoconvective instability in a horizontal porous cavity saturated with cold water. Int. J. Heat Mass Transfer **42**, 4487–4500 (1999)
Marimbordes, T., Ould El Moctar, A., Peerhossaini, H.: Active control of natural convection in a fluid layer with volume heat dissipation. Int. J. Heat Mass Transfer **45**, 667–678 (2002)
Mokhtar, N.F.M., Khalid, I.K.: Stabilization of convective instability in micropolar fluid model by feedback control strategy subjected to internal heat source. Int. J. Math. Models Methods Appl. Sci. **10**, 27–33 (2016)
Mokhtar, N.F.M., Khalid, I.K., Arifin, N.M.: Effect of internal heat generation on Bénard-Marangoni convection in micropolar fluid with feedback control. Icast Contemp. Math. Math. Phys. Their Appl. **435**, 1–17 (2012). https://doi.org/10.88/1742-6596/435/1/012029
Mokhtar, N.F.M., Khalid, I.K., Gani, S.S.A.: Natural convection in a nanofluid layer with feedback control strategy. Int. J. Manag. Appl. Sci. **5**, 30–35 (2017a)
Mokhtar, N.F.M., Khalid, I.K., Siri, Z., Ibrahim, Z.B., Gani, S.S.A.: Control strategy on the double-diffusive convection in a nanofluid layer with internal heat generation. Phys. Fluids **29**, 107105 (2017b)
Muller, G.: Convection and inhomogeneities in crystal growth from the melt. In: Freyhardt, H.C. (ed.) Crystal Growth, Properties and Applications. Springer, Berlin (1988)
Nanjundappa, C.E., Shivakumara, I.S., Arunkumar, R.: Onset of benard-marangoni ferroconvection with internal heat generation. Microgravity Sci. Technol. **23**, 29–39 (2011)
Nield, D.A.: Effects of a magnetic field on streamlines in Bénard convection cells induced by surface tension and buoyancy. ZAMP **17**, 340–342 (1966)
Or, A.C., Kelly, A.C., Cortelezzi, R.E., Speyer, J.L.: Control of long-wavelength Marangoni-Bénard convection. J. Fluid Mech. **387**, 321–341 (1999)
Rayleigh, L.: On convection currents in a horizontal layer of fluid when the higher temperature is in the other side. Philo Mag. **32**, 529–543 (1916)
Roberts, P.H.: Convection in horizontal layers with internal heat generation. Theory J. Fluid Mech. **30**, 33–49 (1967)
Sparrow, E.M., Goldstein, R.J., Jonsson, V.K.: Thermal instability in a horizontal fluid layer: effect of boundary conditions and non-linear temperature profile. J. Fluid Mech. **18**, 513–529 (1964)
Tang, J.: Active Control of Rayleigh-Bénard Convection. PhD thesis, University of Pennsylvania (1996)
Tang, J., Bau, H.H.: Stabilization of the no-motion state in Rayleigh Bénard convection through the use of feedback control. Phys. Rev. Lett. **70**, 1795–1798 (1993)
Tang, J., Bau, H.H.: Stabilization of the no-motion state in of a horizontal fluid layer heated from below with Joule heating. J. Heat Transfer **117**, 329–333 (1995)
Tritton, D.J., Zarraga, M.N.: Convection in horizontall layers with internal heat generation. Exp. J. Fluid Mech. **30**, 21–31 (1967)
Watson, P.: Classical cellular convection with a spatial heat source. J. Fluid Mech. **32**, 399–411 (1968)
Weerakoon, S.: Numerical solution of nonlinear equations in the absence of the derivative. J. Nat. Sci. Coun. Sri Lanka **24**, 309–318 (1996)
Wilson, S.K.: The effect of a uniform magnetic field on the onset of steady Marangoni convection in a layer of conducting fluid. Q. J. Mech. Appl. Math. **46**, 211–248 (1993)
Wilson, S.K.: The effect of a uniform magnetic field on the onset of steady Marangoni convection in a layer of conducting fluid with a prescribed heat flux at its lower boundary. Phys. Fluid **6**, 3591–3600 (1994)